nature physics

LETTERS

PUBLISHED ONLINE: 1 FEBRUARY 2016 | DOI: 10.1038/NPHYS3632

On the growth and form of cortical convolutions

Tuomas Tallinen[1*†], Jun Young Chung[2,3†], François Rousseau[4], Nadine Girard[5,6], Julien Lefèvre[7,8] and L. Mahadevan[2,3,9,10*]

The rapid growth of the human cortex during development is accompanied by the folding of the brain into a highly convoluted structure[1–3]. Recent studies have focused on the genetic and cellular regulation of cortical growth[4–8], but understanding the formation of the gyral and sulcal convolutions also requires consideration of the geometry and physical shaping of the growing brain[9–15]. To study this, we use magnetic resonance images to build a 3D-printed layered gel mimic of the developing smooth fetal brain; when immersed in a solvent, the outer layer swells relative to the core, mimicking cortical growth. This relative growth puts the outer layer into mechanical compression and leads to sulci and gyri similar to those in fetal brains. Starting with the same initial geometry, we also build numerical simulations of the brain modelled as a soft tissue with a growing cortex, and show that this also produces the characteristic patterns of convolutions over a realistic developmental course. All together, our results show that although many molecular determinants control the tangential expansion of the cortex, the size, shape, placement and orientation of the folds arise through iterations and variations of an elementary mechanical instability modulated by early fetal brain geometry.

The convoluted shape of the human cerebral cortex is the result of gyrification that begins after mid-gestation[1,2] (Fig. 1a); before the sixth month of fetal life, the cerebral surface is smooth. The first sulci appear as short isolated lines or triple junctions during the sixth month. These primary sulci soon elongate and branch, and secondary and tertiary sulci form, resulting in a complex pattern of gyri and sulci at birth. Some new sulci develop after birth, further complicating the pattern. Although the course and patterns of gyrification vary across individuals, the primary gyri and sulci have characteristic locations and orientations[16].

Gyrification is, however, not unique to humans, and also exists in a range of primates and other species[17,18]. It has evolved as an efficient way of packing a large cortex into a relatively small skull with natural advantages for information processing[17,19]. Thus, although the functional rationale for gyrification is clear, the physiological mechanism behind gyrification has been unclear. Hypotheses include gyrogenetic theories[4,20] proposing that biochemical prepatterning of the cortex controls the rise of gyri, and the axonal tension hypothesis[21] proposing that axons in white matter beneath the cortex draw together densely interconnected cortical regions to form gyri. There is, however, no evidence of prepatterning that matches gyral patterns, nor is there evidence of axonal tension driving gyrification[10]. At present, the most likely hypothesis is also the simplest one: tangential expansion of the cortical layer relative to sublayers generates compressive stress, leading to the mechanical folding of the cortex[9–15,22–25]. This mechanical folding model produces realistic sizes and shapes of gyral and sulcal patterns[15] that are presumably modulated by brain geometry[26], but the hypothesis has not been tested before with real three-dimensional (3D) fetal brain geometries in a developmental setting. Here we substantiate and quantify this notion using both physical and numerical models of the brain, guided by the use of 3D magnetic resonance images (MRI) of a smooth fetal brain as a starting point.

We construct a physical simulacrum of brain folding by taking advantage of the observation that soft physical gels swell superficially when immersed in solvents. This swelling relative to the interior puts the outer layers of the gel into compression, yielding surface folding patterns qualitatively similar to sulci and gyri[15]. An MRI image of a smooth fetal brain at gestational week (GW) 22 (Fig. 1b; see Supplementary Methods) serves as a template for a 3D-printed cast of the brain. A mould of this form allows us to create a gel-brain (mimicking the white matter) that is then coated with a thin layer of elastomer gel (mimicking the cortical grey matter layer). When this composite gel is immersed in a solvent (see Supplementary Methods) it swells starting at the surface; this leads to superficial compression and the progressive formation of cusped sulci and smooth gyri in the cortex similar in both morphology and relative timing to those seen in real brains (Fig. 1c and Supplementary Movie 1). We note that although the mechanical creasing or sulcification instability is due to the swelling-induced compression, the effect is convoluted by the complex curvature of the initial shape.

To obtain a more quantitative assessment of this process, we carry out a numerical simulation of the developing brain constructed using the same 3D fetal brain MRI (Fig. 1d) as an initial condition for the growth of a soft elastic tissue model of the brain. The model assumes that a cortical layer of thickness h is perfectly adhered to a white matter core and grows with a prescribed tangential expansion ratio g, with both tissues assumed to be soft neo-Hookean elastic solids with similar elastic moduli (see Supplementary Methods). Combining these facts with the known overall isometric growth of the brain[3] yields a differential-strain-based elastic model of brain growth that we solve numerically using custom finite-element methods[15]. For problem parameters, we note that from GW 22 to adulthood (Supplementary Fig. 1) there is an approximately

[1]Department of Physics and Nanoscience Center, University of Jyvaskyla, FI-40014 Jyväskylä, Finland. [2]Paulson School of Engineering and Applied Sciences, Harvard University, Cambridge, Massachusetts 02138, USA. [3]Wyss Institute for Biologically Inspired Engineering, Harvard University, Cambridge, Massachusetts 02138, USA. [4]Institut Mines-Telecom, Telecom Bretagne, INSERM U1101 LaTIM, 29609 Brest, France. [5]Aix-Marseille Université, CRMBM UMR 7339, 13385 Marseille, France. [6]Service de Neuroradiologie, Hópital de la Timone, 13005 Marseille, France. [7]Aix-Marseille Université, CNRS, ENSAM, Université de Toulon, LSIS UMR 7296, 13397 Marseille, France. [8]Institut de Neurosciences de la Timone UMR 7289, Aix Marseille Université, CNRS, 13385 Marseille, France. [9]Departments of Organismic and Evolutionary Biology, and Physics, Harvard University, Cambridge, Massachusetts 02138, USA. [10]Kavli Institute for Nanobio Science and Technology, Harvard University, Cambridge, Massachusetts 02138, USA. †These authors contributed equally to this work. *e-mail: tuomas.tallinen@jyu.fi; lm@seas.harvard.edu

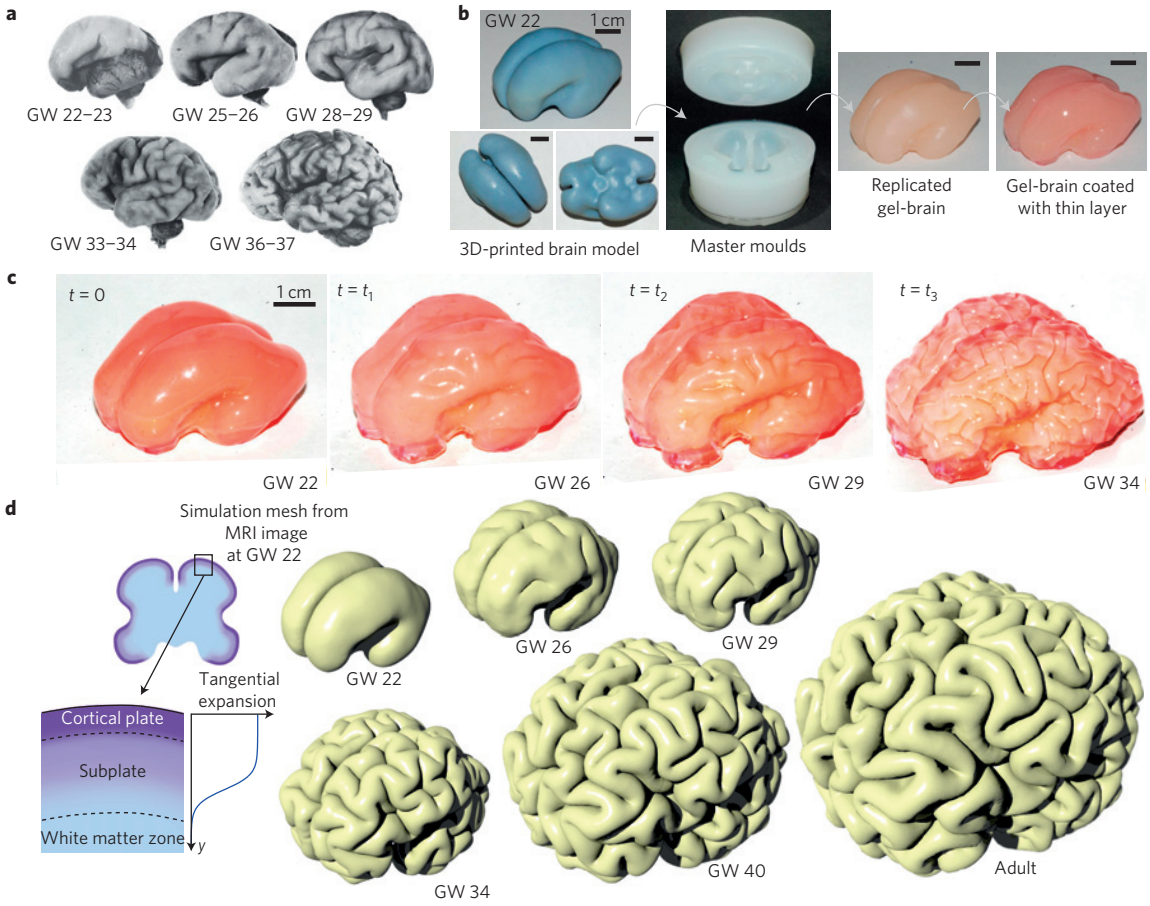

Figure 1 | Physical mimic and numerical simulation of tangential cortical expansion. a, Gyrification of the human brain during the latter half of gestation (photographs from ref. 1, adapted with permission from Elsevier). **b**, A 3D-printed model of the brain is produced from a 3D MRI image of a smooth fetal brain and then used to create a pair of negative silicone moulds for casting. To mimic the constrained growth of the cortex, a replicated gel-brain (white matter) is coated with a thin layer of gel (cortex) that swells by absorbing a solvent (hexanes) over time t ($t_1 \approx 4$ min, $t_2 \approx 9$ min, $t_3 \approx 16$ min). **c**, The layered gel progressively evolves into a complex pattern of sulci and gyri during the swelling process. **d**, A simulation starting from a smooth fetal brain shows gyrification as a result of uniform tangential expansion of the cortical layer. The brain is modelled as a soft elastic solid and a relative tangential expansion is imposed on the cortical layer as shown at left, and the system allowed to relax to its elastic equilibrium.

20-fold increase in brain volume (approximately 60 ml to 1,200 ml), and a 30-fold increase in cortical area (approximately 80 cm^2 to 2,400 cm^2), whereas the expanding cortical layer changes little, with a typical thickness of 2.5 mm in the undeformed reference state (the deformed thickness is about 3 mm). In physiological terms, we thus assume that tangential expansion during the fetal stage extends through the cortical plate (which has a thickness of about 1–1.5 mm at GW 22) and decays rapidly in the subplate (Fig. 1d, left). The subplate diminishes during gyrification while the cortical plate thickens and develops into the cerebral cortex[1,3], so that in the simulated adult brain the expanding layer corresponds to the cerebral cortex (which is about 3 mm thick in adults).

Our simple parametrization of brain growth leads to emergence of gyrification in space and time along a course similar to real brains (Fig. 1d and Supplementary Movie 2): gyrification is initiated through the formation of isolated line-like sulci (GW 26), which elongate and branch, establishing most of the patterns before birth (GW 40). After birth, brain volume still increases nearly threefold, and during this time our model shows that the gyral patterns are modified mainly by the addition of some new bends to existing gyri in agreement with longitudinal morphological analyses[27]. The characteristic spatiotemporal appearance of these convolutions—rounded gyri between sharply cusped sulci in a mixture of threefold junctions and S-shaped bends[28]—is a direct consequence of the mechanical instability induced by constrained cortical expansion. Physically, the similar stiffness of the cortex and sublayers implies that gyrification arises as a non-trivial combination of a smooth linear instability[29] and a nonlinear sulcification instability[30–32].

Sections of the physically and numerically simulated brains shown in Fig. 2a,b exhibit a bulging of gyri and deepening of sulci in a sequence resembling the observations from MRI sections. Our simulations of gyrification driven by constrained cortical expansion allow us to also measure the gyrification index (GI, defined as the ratio of the surface contour length to that of the convex hull, determined here from coronal sections as described in ref. 3). We see that there is a clear increase in the GI with developing brain volume in agreement with observations (Fig. 2c). The GI arising from our numerical simulation reaches 2.5, matching observations of adult brains. A different measure of the GI based on the cortical surface area rather than that of sections shows that the simulated adult brain has a cortical area that is approximately four times the exposed cortical area (Supplementary Fig. 1). For comparison, we also section our physical gel simulacrum that swells from an initial unpatterned state (GI = 1.07, GW 22) and see that as a function of swelling, the GI increases to about 1.55, a modest increase associated with an approximately twofold increase in brain volume, the latter state corresponding to roughly GW 30–34 (Fig. 2c and Supplementary Fig. 2). The ultimate limiting factor in our physical experiments is the inability for our gel to swell and increase its volume 20-fold like in fetal brains.

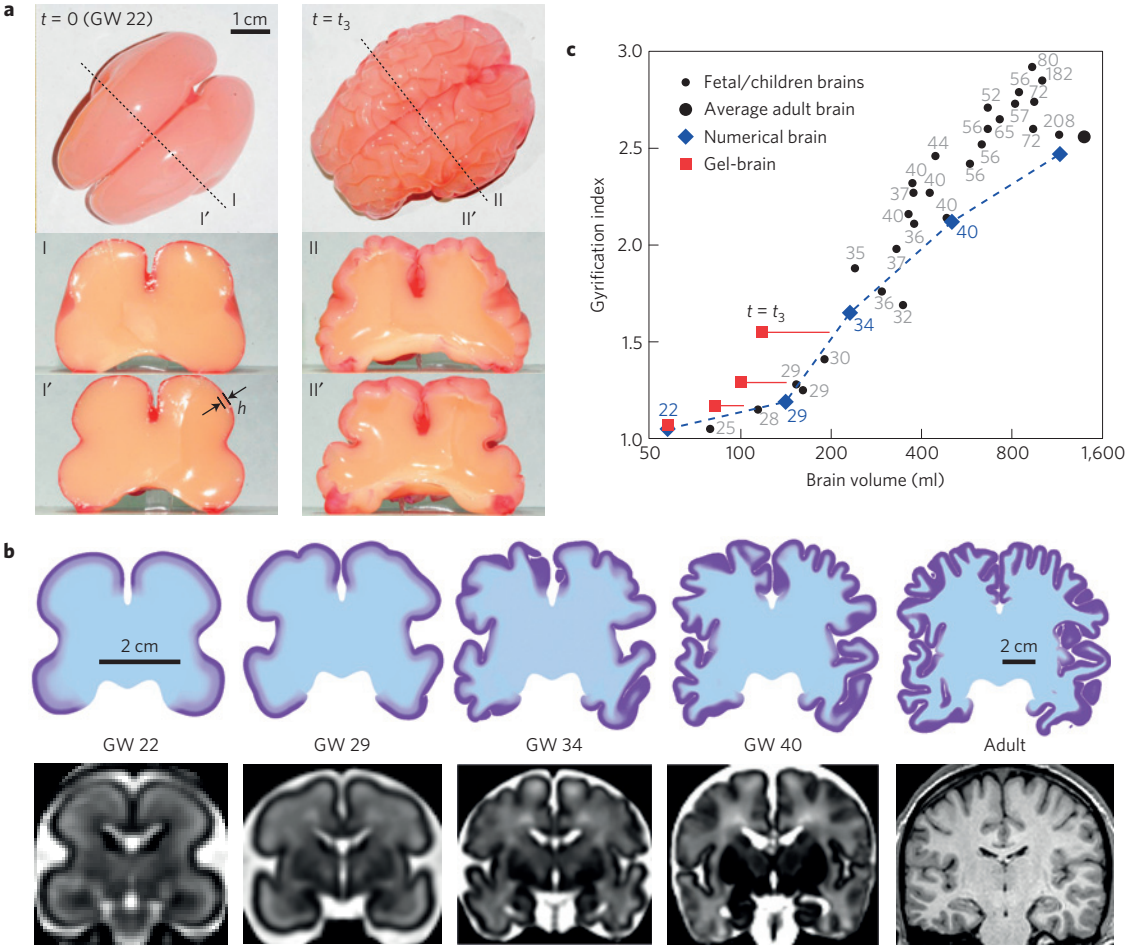

Figure 2 | Sectional views of model brains during convolutional development. a, Planform and cross-sectional images of a physical gel-brain showing convolutional development during the swelling (folding) process that starts from an initially smooth shape (left panels) to a moderately convoluted shape (right panels). **b**, The coronal sections of the simulated brain (top panels) with comparisons to corresponding MRI sections[35,39]. **c**, Gyrification index as a function of brain size for real brains (data from refs 3,40), a numerically simulated brain, and a physical gel-brain. Gestational week is indicated for fetal and children brains. The initial volume of the gel-brain (≈34 ml) is scaled to match that of the simulated brain (≈57 ml). Note that in the gel experiments only the outer layer swells and therefore the volume grows less than in real brains.

Having seen that our physical and numerical experiments can capture the overall qualitative picture of how gyri form, we now turn to the question of the role of brain geometry and mechanical stresses in controlling the placement and orientations of the major and minor sulci and gyri. In Fig. 3a, we show the field of the simulated compressive stress just before the primary sulci form. Although cortical growth in our model is relatively uniform in space, the curvature of the surface is not. This yields a non-uniform stress field in the cortical layer. Thus, compressive stresses are reduced in the vicinity of highly curved convex regions, so that the first sulci appear at weakly curved or concave regions in our simulations, consistent with observations in fetal brains[1,16]. Furthermore, compression-induced sulci should favour their alignment perpendicular to the largest compressive stress, and indeed directions of the largest compressive stress in our model are perpendicular to the general orientations of primary gyri and sulci (Fig. 3a). Figure 3b shows that the first generations of sulci form perpendicular to the maximum compressive stress in real and simulated model brains; this correlation is particularly clear for the primary sulci in real brains.

Although the shape of the initially smooth fetal brain is described by the curvature of its surface, cortical growth eventually couples the curvature and mechanical stress in non-trivial ways. In Supplementary Fig. 3 we compare the stress field and curvature at the cortical surface just before the first sulci form, and see that in highly curved regions the maximum compressive stress is perpendicular to the highest (convex) curvature. However, this does not hold at the ellipsoidal surfaces of the frontal and temporal lobes; these lobes elongate and bend towards each other as a result of cortical growth (Supplementary Fig. 3; Supplementary Movie 1 shows the analogue in our gel experiments). This reduces the compressive stress in the direction of elongation and bending, which in turn is reflected in the dominant orientations of the frontal and temporal gyri.

Although the global brain shape directs the orientations of the primary gyri, the finer details of the gyrification patterns are sensitive to variations in the initial geometry. In Fig. 3c we see that the patterns of gyri and sulci on a physical gel-brain exhibit some deviations from perfect bilateral symmetry. The hemispheres are not identical in real brains either, but we note that in our models artefacts from imaging, surface segmentation, and sample preparation can cause the two hemispheres to differ more than in reality. The sequential patterns emerging from the folding (swelling) and unfolding (drying) process also show some degree of variations (Supplementary Fig. 4), but this process is highly repeatable; indeed, the resulting gyral patterns are found to be robust and reproducible on multiple repetition of the experiment with the same gel-brain sample (lower left of Fig. 3c). The folding patterns vary in detail across samples (Supplementary Fig. 4), but they share general

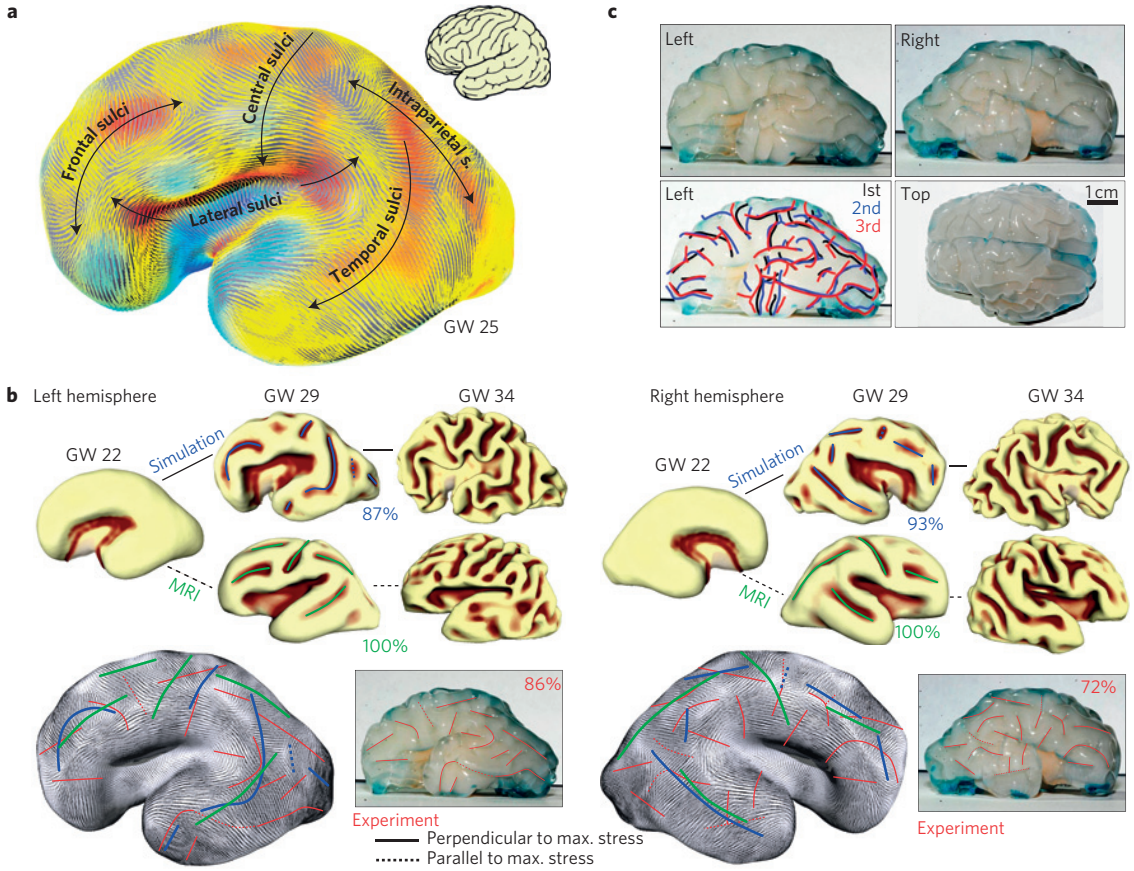

Figure 3 | Mechanical stress orients convolutions. a, A simulated stress field just before the onset of gyrification. Lines indicate the direction of maximum compressive stress and colour indicates the magnitude of the stress (red, high). General directions of primary sulci are indicated using solid arrows. A simplified scheme of the human brain[17] indicating the general orientations of sulci is shown at the top right. **b**, View of the first generations of sulci in a numerical simulation, in real brains (MRI, different brains for GW 22, 29 and 34), and a physical gel-brain on both hemispheres, with the former two showing the inner surfaces of cortical plates. The sulcal lines (blue, simulation; green, real brain; red, experiment) are superposed on the simulated vector fields of maximum compressive stress at GW 25 and show that most sulci form perpendicular to the direction of maximum compressive stress (solid and dotted lines are perpendicular (angle $>45°$) and parallel (angle $<45°$) to the stress vector field, respectively). The percentage of sulcal length perpendicular to the stress vectors is indicated in each case. **c**, A folded gel-brain showing a certain lack of symmetry between the right and left hemispheres. The panel on the lower left shows nearly overlapping sets of sulcal lines obtained from three repeated tests with the same gel-brain (see Supplementary Fig. 4).

similarities in terms of the alignment of sulci and gyri and the inter-sulcal spacing. These experimentally derived findings corroborate numerical results; in Supplementary Fig. 5 we see the extent of variations associated with imperfections, by comparing the left and right hemispheres of the simulated brain when the simulation has been run forwards (folding) or backwards (unfolding) in time. In Supplementary Fig. 6 we compare the simulated folding of two different brains (starting from MRI images of different fetal brains) and see that the patterns in both brains are consistent with the scheme depicted in Fig. 3a.

We quantify our qualitative comparison of the similarities between real and simulated brains in Fig. 4 using morphometric techniques. Conformal mapping of the curvature vector fields (see Supplementary Methods) allows for a visual (Fig. 4a) as well as quantitative comparison (Fig. 4b), which indicates similar average alignments of curvature fields, and thus folds, in both the simulated and real brains. As a final comparison, in Fig. 4c,d we identify visually many of the named primary gyri[1] from the simulated brains and compare to a real fetal brain at a similar stage, and note that our simulations can capture many of the trends quantitatively.

All together, by combining physical experiments and numerical simulations originating with initially smooth 3D fetal brain geometries, we have quantified a simple mechanical folding scenario for the development of convolutions in the fetal brain. Our physical gel model shows that we can capture the qualitative features of the folding patterns that are driven by a combination of surface swelling and surface geometry, setting the stage for how biology can build on this simple physical pattern-forming instability. Our numerical model is fully quantitative, based on parameters that are known by simple measurements: cortical thickness, white and grey matter tissue stiffness, brain growth and relative tangential expansion of the cortex. Together, they show that gyrification is an inevitable mechanical consequence of constrained cortical expansion; patterned gyri and sulci that are consistent with observations arise even in the absence of any patterning of cortical growth. Furthermore, although cortical expansion and brain shape couple to guide placement and orientation of gyri, the finer details of the patterns, on scales comparable to the cortical thickness, are sensitive to geometrical and mechanical perturbations. Real brains are likely to have small inter-individual variations in shape, tissue properties and growth rates, and the sensitivity of mechanical folding to such small variations could explain the variability of gyrification patterns, although the primary convolutions are consistently reproducible in their location and timing.

Our organ-level approach complements the recent emphases on the many molecular determinants underlying neuronal cell size and shape, as well patterns in their proliferation and migration[4,24]. These variables are functions of time and space in the cortex

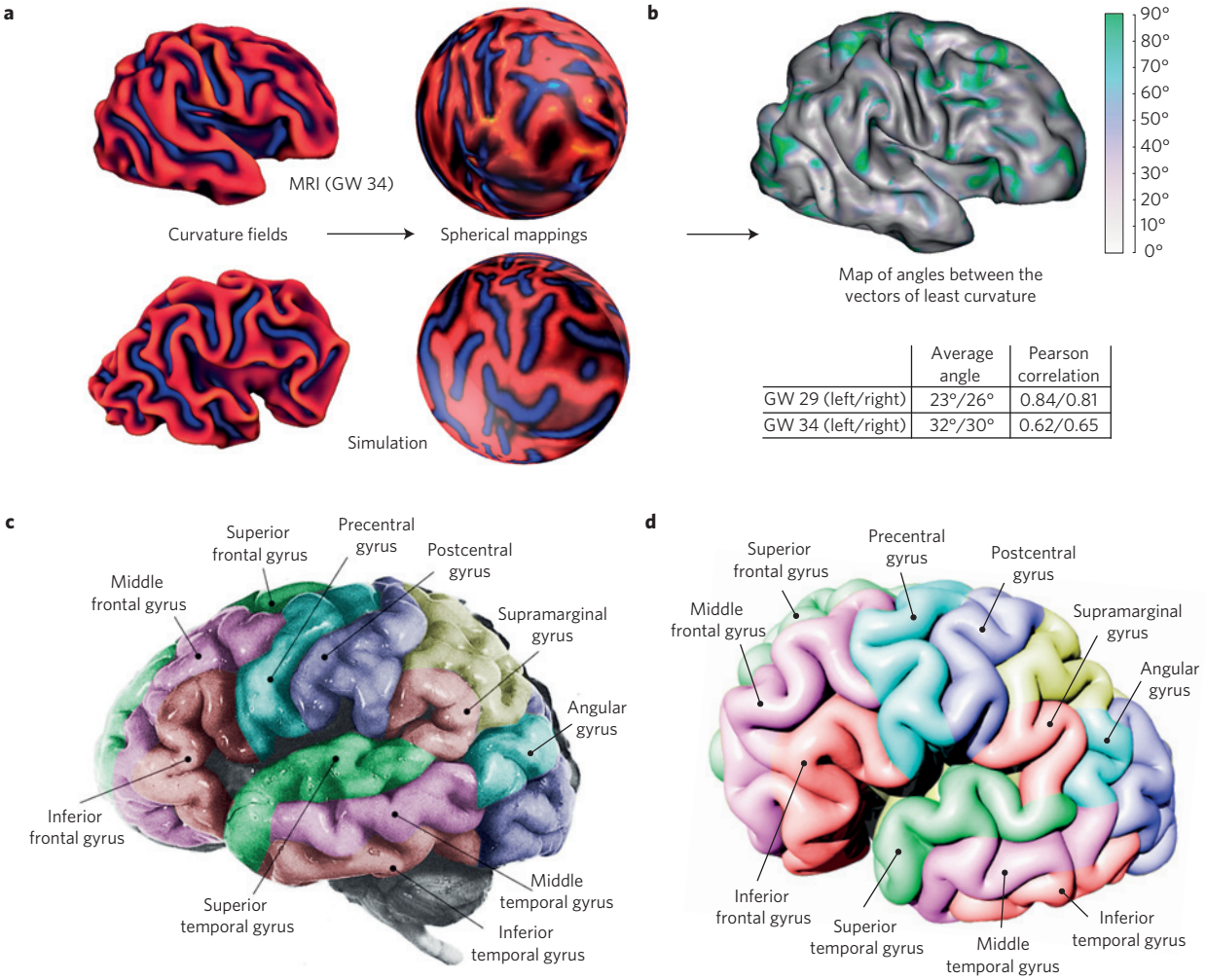

	Average angle	Pearson correlation
GW 29 (left/right)	23°/26°	0.84/0.81
GW 34 (left/right)	32°/30°	0.62/0.65

Figure 4 | Comparison of real and simulated folding patterns. a, Conformal spherical mappings (see Supplementary Methods) of inner cortical surfaces of real and simulated fetal brains. **b**, A map of angles between the vectors of the least absolute curvature of the real and simulated brain surfaces. The angle field is computed in the spherical domain and mapped back on the real brain. In grey regions the curvature directions match and in green regions they are mismatched. Average angles and Pearson correlations between real and simulated curvature fields at GW 29 and 34 are given in the table (details in Supplementary Methods). **c**, All notable gyri have formed by GW 37 as identified on a real fetal brain (adapted from ref. 1 with permission from Elsevier). **d**, Analogous regions shown in a simulated brain driven by constrained cortical expansion. In both cases, the colouring is based on visual identification of the major gyri.

and the sub-ventricular zone, but ultimately feed into just two physical parameters for a given initial brain shape: relative cortical expansion and the ratio of cortical thickness/brain size[15]. By grounding our study on observations of fetal brain development, where these parameters are known, our work provides a quantitative basis for the proximal biophysical cause of gyrification. Our results can serve as a template for physically based morphometric studies that characterize the developing geometry of the brain surface[33–35] in terms of variations in initial brain shape and cortical expansion. Additionally, our study sets the biophysical basis for an understanding of a range of functional neurological disorders linked to structural cortical malformations[4,36] that are associated with neurogenesis and brain size (for example, ASPM and CENPJ for microcephaly[4,37]) and cell migration and cortex thickness (for example, GPR56 for polymicrogyria[6] and RELN for lissencephaly[38]). With this information, a natural next step is to link the molecular determinants to the macroscopic mechanics quantitatively, and ask how brain shape and function are mutually co-regulated.

Received 27 September 2015; accepted 9 December 2015; published online 1 February 2016

References

1. Griffiths, P. D., Reeves, M., Morris, J. & Larroche, J. *Atlas of Fetal and Neonatal Brain MR Imaging* (Mosby, 2010).
2. Girard, N. & Gambarelli, D. *Normal Fetal Brain: Magnetic Resonance Imaging. An Atlas with Anatomic Correlations* (Label Production, 2001).
3. Armstrong, E., Scleicher, A., Omran, H., Curtis, M. & Zilles, K. The ontogeny of human gyrification. *Cereb. Cortex* **5,** 56–63 (1995).
4. Sun, T. & Hevner, R. F. Growth and folding of the mammalian cerebral cortex: from molecules to malformations. *Nature Rev. Neurosci.* **15,** 217–232 (2014).
5. Lui, J. H., Hansen, D. V. & Kriegstein, A. R. Development and evolution of the human neocortex. *Cell* **146,** 18–36 (2011).
6. Bae, B. *et al.* Evolutionarily dynamic alternative splicing of GPR56 regulates regional cerebral cortical patterning. *Science* **343,** 764–768 (2014).
7. Rash, B. G., Tomasi, S., Lim, H. D., Suh, C. Y. & Vaccarino, F. M. Cortical gyrification induced by fibroblast growth factor 2 in the mouse brain. *J. Neurosci.* **33,** 10802–10814 (2013).
8. Reillo, I., de Juan Romero, C., Garcia-Cabezas, M. A. & Borrell, V. A role of intermediate radial glia in the tangential expansion of the mammalian cerebral cortex. *Cereb. Cortex* **21,** 1674–1694 (2011).
9. Richman, D. P., Stewart, R. M., Hutchinson, J. W. & Caviness, V. S. Jr Mechanical model of brain convolutional development. *Science* **189,** 18–21 (1975).
10. Xu, G. *et al.* Axons pull on the brain, but tension does not drive cortical folding. *J. Biomech. Eng.* **132,** 071013 (2010).

11. Toro, R. & Burnod, Y. A morphogenetic model for the development of cortical convolutions. *Cereb. Cortex* **15,** 1900–1913 (2005).
12. Nie, J. *et al.* A computational model of cerebral cortex folding. *J. Theor. Biol.* **264,** 467–478 (2010).
13. Budday, S., Raybaud, C. & Kuhl, E. A mechanical model predicts morphological abnormalities in the developing human brain. *Sci. Rep.* **4,** 5644 (2014).
14. Bayly, P. V., Okamoto, R. J., Xu, G., Shi, Y. & Taber, L. A. A cortical folding model incorporating stress-dependent growth explains gyral wavelengths and stress patterns in the developing brain. *Phys. Biol.* **10,** 016005 (2013).
15. Tallinen, T., Chung, J. Y., Biggins, J. S. & Mahadevan, L. Gyrification from constrained cortical expansion. *Proc. Natl Acad. Sci. USA* **111,** 12667–12672 (2014).
16. Ono, M., Kubik, S. & Abernathey, C. D. *Atlas of the Cerebral Sulci* (Georg Thieme Verlag, 1990).
17. Striedter, G. F. *Principles of Brain Evolution* (Sinauer Associates, 2005).
18. Mota, B. & Herculano-Houzel, S. Cortical folding scales universally with surface area and thickness, not number of neurons. *Science* **349,** 74–77 (2015).
19. Zilles, K., Palomero-Gallagher, N. & Amunts, K. Development of cortical folding during evolution and ontogeny. *Trends Neurosci.* **36,** 275–284 (2013).
20. Welker, W. Why does cerebral cortex fissure and fold: a review of determinants of gyri and sulci. *Cereb. Cortex* **8,** 3–136 (1990).
21. van Essen, D. C. A tension based theory of morphogenesis and compact wiring in the central nervous system. *Nature* **385,** 313–318 (1997).
22. Ronan, L. *et al.* Differential tangential expansion as a mechanism for cortical gyrification. *Cereb. Cortex* **24,** 2219–2228 (2014).
23. Holland, M. A., Miller, K. E. & Kuhl, E. Emerging brain morphologies from axonal elongation. *Ann. Biomed. Eng.* **43,** 1640–1653 (2015).
24. Striedter, G. F., Srinivasan, S. & Monuki, E. S. Cortical folding: when, where, how and why? *Annu. Rev. Neurosci.* **38,** 291–307 (2015).
25. Bayly, P. V., Taber, L. A. & Kroenke, C. D. Mechanical forces in cerebral cortical folding: a review of measurements and models. *J. Mech. Behav. Biomed.* **29,** 568–581 (2013).
26. Todd, P. H. A geometric model for the cortical folding pattern of simple folded brains. *J. Theor. Biol.* **97,** 529–538 (1982).
27. Meng, Y., Li, G., Lin, W., Gilmore, J. H. & Shen, D. Spatial distribution and longitudinal development of deep cortical sulcal landmarks in infants. *NeuroImage* **100,** 206–218 (2014).
28. Li, K. *et al.* Gyral folding pattern analysis via surface profiling. *NeuroImage* **52,** 1202–1214 (2010).
29. Biot, M. A. *Mechanics of Incremental Deformations* (John Wiley, 1965).
30. Hohlfeld, E. & Mahadevan, L. Unfolding the sulcus. *Phys. Rev. Lett.* **106,** 105702 (2011).
31. Hohlfeld, E. & Mahadevan, L. Scale and nature of sulcification patterns. *Phys. Rev. Lett.* **109,** 025701 (2012).
32. Tallinen, T., Biggins, J. & Mahadevan, L. Surface sulci in squeezed soft solids. *Phys. Rev. Lett.* **110,** 024302 (2013).
33. Toro, R. *et al.* Brain size and folding of the human cerebral cortex. *Cereb. Cortex* **18,** 2352–2357 (2008).
34. Germanaud, D. *et al.* Larger is twistier: spectral analysis of gyrification (SPANGY) applied to adult brain size polymorphism. *NeuroImage* **63,** 1257–1272 (2012).
35. Lefèvre, J. *et al.* Are developmental trajectories of cortical folding comparable between cross-sectional datasets of fetuses and preterm newborns? *Cereb. Cortex* http://dx.doi.org/10.1093/cercor/bhv123 (2015).
36. Aronica, E., Becker, A. J. & Spreafico, R. Malformations of cortical development. *Brain Pathol.* **22,** 380–401 (2012).
37. Bond, J. *et al.* A centrosomal mechanism involving CDK5RAP2 and CENPJ controls brain size. *Nature Genet.* **37,** 353–355 (2005).
38. Hong, S. E. *et al.* Autosomal recessive lissencephaly with cerebellar hypoplasia is associated with human RELN mutations. *Nature Genet.* **26,** 93–96 (2000).
39. Serag, A. *et al.* Construction of a consistent high-definition spatio-temporal atlas of the developing brain using adaptive kernel regression. *NeuroImage* **59,** 2255–2265 (2012).
40. Zilles, K., Armstrong, E., Scleicher, A. & Kretschmann, H. The human pattern in gyrification in the cerebral cortex. *Anat. Embryol.* **170,** 173–179 (1988).

Acknowledgements

We thank CSC—IT Center for Science, Finland, for computational resources and J. C. Weaver for help with 3D printing. This work was supported by the Academy of Finland (T.T.), Agence Nationale de la Recherche (ANR-12-JS03-001-01, "Modegy") (N.G. and J.L.), the Wyss Institute for Biologically Inspired Engineering (J.Y.C. and L.M.), and fellowships from the MacArthur Foundation and the Radcliffe Institute (L.M.).

Author contributions

T.T., J.Y.C. and L.M. conceived the model and wrote the paper. T.T. developed and performed the numerical simulations. J.Y.C. developed and performed the physical experiments. J.L. developed and performed the morphometric analyses. F.R., N.G. and J.L. provided MRI images and provided feedback on the manuscript. T.T. and L.M. coordinated the project.

Additional information

Supplementary information is available in the online version of the paper. Reprints and permissions information is available online at www.nature.com/reprints. Correspondence and requests for materials should be addressed to T.T. or L.M.

Competing financial interests

The authors declare no competing financial interests.

nature physics

SUPPLEMENTARY INFORMATION

DOI: 10.1038/NPHYS3632

On the growth and form of cortical convolutions

1. METHODS

1.1. Physical Model

The initial geometry of the physical gel brain is constructed using 3D printing and replica molding techniques based on a T2-weighted motion corrected 3D MRI image of a smooth fetal brain at GW 22 (Fig. 1b). A 3D brain model is first printed as a single piece of plastic using a 3D printer (Connex500, Stratasys Ltd.) and subsequently used to create a pair of negative molds made of a supersoft silicone (Ecoflex, Smooth-On Co.). These master molds are then used to cast the core of a gel brain (white matter) with a lightly cross-linked poly(dimethylsiloxane) (PDMS) elastomer (Sylgard 184, Dow Chemical Co.). To accomplish this, the two-part PDMS prepolymer is thoroughly mixed in a 45:1 mass ratio of base to cross-linker and poured into the molds. The mixture is left at room temperature for a few hours to allow trapped air bubbles to escape and then cured at 75 °C in a relatively short period of time (about 30 min) in order to produce a partially cured contact surface. After cooling, a replicated PDMS core is carefully extracted from the molds. The surface of the partially cured PDMS is sticky and thus is used to provide strong bonding with the outer layer being applied.

The outer layer of a gel brain (cortical layer) is fabricated by a layer-by-layer drop-casting method, in which the thickness of each layer is controlled by adjusting the amount and viscosity of uncured PDMS mixture deposited on the pre-prepared brain core in a pre-heated oven. Briefly, PDMS base is mixed homogeneously with cross-linker at a 35:1 mass ratio and the mixture is vacuum degassed to eliminate air bubbles. Drops of the mixture are then deposited and uniformly spread onto the entire surface of the brain core (except for a central portion of the bottom; see Fig. S2), resulting in a layer thickness of the order of hundreds of micrometers. After deposition, a layered brain core is partially cured at 75 °C for 20 min to ensure bonding with the subsequent layer. This whole process is repeated several times until the desired thickness of the outer layer (about 1 mm) is reached. Finally, the bottom portion of the uncovered brain core is coated with a thin layer of PDMS with a mass ratio of 10:1 base to cross-linker, and the whole specimen is completely cured at 75 °C overnight.

The dimensions of the fabricated layered gel brain are shown in Fig. S2, and the thickness of the cortical layer is determined by the cross-sectional image. Colored pigments are used to enhance the contrast between the cortical layer and the brain core because the cross-linked PDMS is optically transparent. The shear moduli of the brain core, and the cortical and bottom layers in their fully cured state are ≈15 kPa, ≈40 kPa, and ≈1 MPa, respectively, which are measured by a cone-and-plate rheometer (Anton Paar Physica MCR 501, the cortical layer is made initially slightly stiffer than the core to account for its softening during swelling, see below). All these parts of the gel brain are shown as an elastic solid, as reported in ref. [1].

To mimic the constrained growth of the cortex as seen in normal fetal brain development, we

DOI: 10.1038/NPHYS3632

consider the swelling of a layered gel brain immersed in a compatible organic solvent. Hexanes is selected on the basis of its superior swelling ability for PDMS [2]. The prepared gel brain is placed in a glass jar filled with hexanes (Sigma-Aldrich) at room temperature for a limited period of time (typically 20–30 min), which is sufficient to cause differential swelling of the outer layer of the gel brain with respect to its core, but short enough to prevent the solvent from penetrating into the brain core. Consequently, the modulus of the outer layer in the swollen state becomes lower than that in the initial dry state, while the modulus of the core remains unchanged. After exposure to the solvent, the swollen gel brain is promptly withdrawn from the glass jar and subsequently imaged with a digital camera equipped with a zoom lens (Fig. 1c). In some cases, the gel brain is dissected along a coronal plane in order to obtain its internal parts (Fig. 2a and Fig. S2).

We consider the case where both cortical layer and core have similar elastic moduli, as established in the previous study [3]. This is accomplished by making the cortical layer slightly stiffer than the core (by utilizing a relatively high percentage of cross-linker for the outer layer as specified above), so that when the layered brain gel is immersed in a solvent the modulus of the outer layer is comparable to that of the core. In addition, a thin layer of a highly cross-linked PDMS (with a greater percentage of cross-linker) is applied onto the bottom portion of the gel brain to minimize its swelling during solvent exposure.

1.2. Computational Model

The simulation geometry is based on a T2-weighted motion corrected MRI of a fetal brain at 22 GW, with an isotropic resolution of about $0.5 \times 0.5 \times 0.5$ mm^3. To create a tetrahedral simulation mesh from the MRI, the cortical surface is first triangulated and the brain volume is meshed uniformly with approximately 10^7 tetrahedrons, yielding at least five layers of tetrahedrons across the cortical thickness. The brain is assumed to be of neo-Hookean hyperelastic material with strain energy density

$$W = \frac{\mu}{2}\left[\mathrm{Tr}(\mathbf{F}\mathbf{F}^{\mathrm{T}})J^{-2/3} - 3\right] + \frac{K}{2}(J-1)^2, \tag{1}$$

where μ is a shear modulus, K is a bulk modulus, $\mathbf{F}$ is a deformation gradient, and $J = \det \mathbf{F}$. We assume $K = 5\mu$, corresponding to a modestly compressible material. To handle extreme deformations of the growing brain matter we use constant strain tetrahedral finite elements with inversion handling [4] and nodal pressure formulation [5]. Contacts at the brain surface are modeled via penalty based vertex-triangle contact processing [6]. Deformation energy of the system is minimized by quasistatic equilibration using an explicit solver. Growth is applied by expanding the sizes of the elements while retaining the mesh topology.

To distinguish between the cortical layer and white matter zone, we apply an indicator function

$$\theta(y) = \frac{1}{1 + e^{10(y/h-1)}} \tag{2}$$

that steps smoothly from the cortical layer ($\theta = 1$) to white matter zone ($\theta = 0$). In eq. (2) y is the distance from surface in material coordinates and h is the cortical thickness. The tangential cortical expansion ratio is $g(y) = 1 + (\sqrt{8} - 1)\theta(y)t$, where $t \in [0, 1]$ parametrizes time, and the corresponding growth tensor is $\mathbf{G} = g(y)\mathbf{I} + [1 - g(y)]\hat{\boldsymbol{n}} \otimes \hat{\boldsymbol{n}}$, where $\hat{\boldsymbol{n}}$ is the surface normal of the

reference state (Fig. 1d and Fig. S1). At $t = 1$ (adult brain) the cortical layer thus has an areal growth by a factor of $g^2 = 8$ relative to the white matter zone in the victitious stress-free state (area expansion in the deformed state is less since the layer is compressed). To account for the observed volume growth during gyrification, the size of the reference state is scaled isotropically such that its longitudinal length is $L = 59/(1 - 0.55t)$ mm (at $t = 0$ $L = 59$ mm as measured from the MRI). The thickness h of the cortical layer relative to L is $h/L = 0.042 - 0.021t$, corresponding approximately to 2.5 mm undeformed thickness. The simulations are mapped to gestational age based on brain size data from ref. [7] (Fig. 2c). Based on measurements [8], we assume that the cortical layer is slightly softer than the white matter zone, with a modulus ratio $\mu_c/\mu_w = 0.86$. The modulus across the domain is $\mu(y) = \theta(y)\mu_c + [1 - \theta(y)]\mu_w$.

To capture the full course of gyrification in a single simulation run as shown in Movie S2, the simulation is run backwards in time. To this end, the adult pattern is first produced by expanding the cortex while its thickness relative to brain size is fixed to the adult value. The brain is then unfolded ($t : 1 \to 0$) with parameters depending on t as described above. When the simulation is run forwards in time ($t : 0 \to 1$), the cortical thickness relative to brain size decreases during simulation, which is problematic toward the end of simulation and leads to metastable states with higher deformation energies in comparison to unfolding simulations. The simulated configurations shown in the main paper are snapshots from the full backward simulation. However, up to modestly gyrified states the folding and unfolding simulations provide similar results (Fig. S5).

1.3. Morphometric Analysis

To perform morphometric analyses of cortical folding patterns of real and simulated brains (shown in Fig. 4), the inner cortical surfaces are modeled as triangular meshes with spherical topologies. Folding patterns are described by curvature fields [9] and for our analysis it suffices to consider only the vector fields corresponding to the minimal curvature in absolute value, since it coincides with the orientation of sulci and gyri. We perform analyses separately for the left and right hemispheres.

To compare quantitatively two cortical surfaces $\mathcal{M}$ and $\mathcal{N}$, we use a spherical parameterization approach which maps a sphere-like surface onto the sphere S^2 by means of the three first non-trivial eigenfunctions of the Laplace-Beltrami operator of the surfaces [10]. This mapping $m : \mathcal{M} \to S^2$ is diffeomorphic and the mappings are aligned by large scale features such as sylvian fissure or internal face, without manually defined landmarks. A vector field $\mathbf{V}$ on $\mathcal{M}$ can be transported onto the sphere by using the pushforward m^* of $\mathbf{V}$. It is classically defined at each point $p \in S^2$ as

$$(m^*\mathbf{V})(p) = (Dm)_{m^{-1}(p)}\mathbf{V}\big[m^{-1}(p)\big]. \tag{3}$$

where Dm is the differential of m and m^{-1} is the inverse transformation of m. Vector fields on $\mathcal{M}$ and $\mathcal{N}$ can thus be transformed onto the sphere so as to obtain at each point two vectors $(m^*\mathbf{V})(p)$ and $(n^*\mathbf{V})(p)$, whose scalar product, and therefore angle, can be obtained via the canonical metric on the sphere expressed in spherical coordinates: $ds^2 = d\theta^2 + \sin^2\theta d\phi^2$. The statistics on angle distributions are complemented in Fig. 4b by the Pearson correlation coefficient computed between all the components of the two vector fields.

DOI: 10.1038/NPHYS3632

2. SUPPLEMENTARY FIGURES

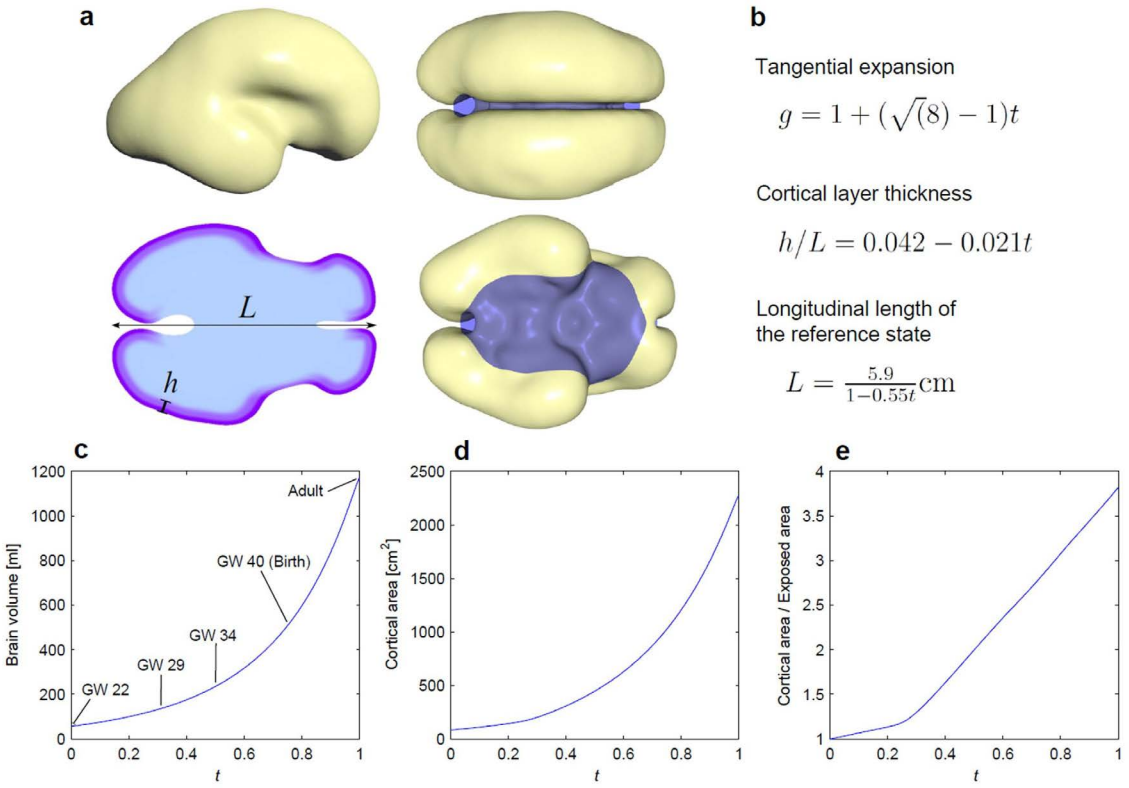

FIG. S1. **Geometry, parametrization, and time evolution of the simulated brain.** (**a**) Side, top and bottom views and a horizontal section of the initial geometry which is also the reference state of the simulation. Surface enclosed by the blue ellipsoid in the top and bottom views is excluded from the growing cortical layer. The longitudinal length L and cortical thickness h are indicated in the horizontal section. (**b**) Parametrization of the model. (**c**) Brain volume as a function of time t. Estimated correspondence to gestational age is indicated. (**d**) Cortical area as a function of t. (**e**) Cortical area relative to exposed area as a function t. Exposed area is defined as the area of a smooth initial geometry that is scaled to (approximately) cover the gyrificated brain.

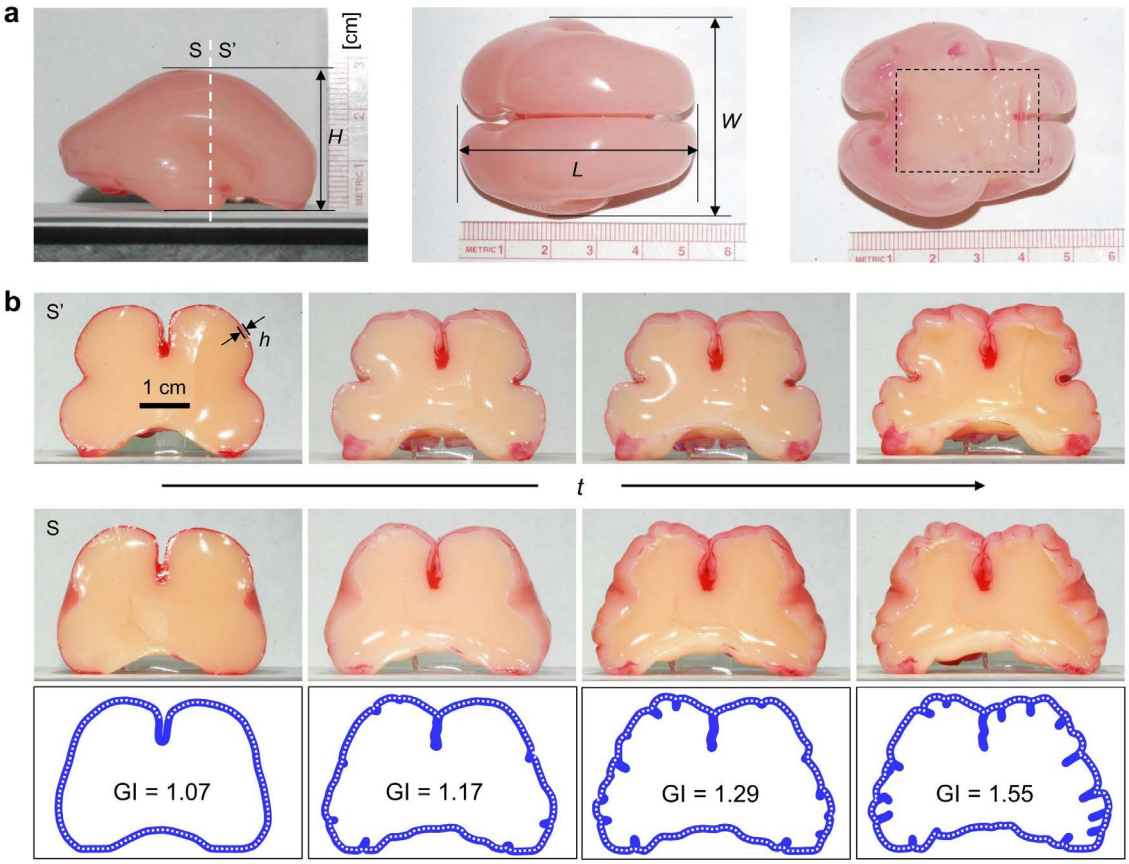

FIG. S2. **Geometry and time evolution of the physical gel brain.** (**a**) Side, top, and bottom views of the initial geometry, showing a layered gel brain with longitudinal length L of ≈5 cm, lateral width W of ≈4 cm, and height H of ≈3 cm. The surface within the dotted box in the bottom view is excluded from the swelling cortical layer. Note that a different colored pigment is used for the cortex to differentiate it from the core white matter. (**b**) Representative coronal cross-sections of a gel brain at different points in time t (top and middle panels). The rise of gyri and the deepening of sulci appear in a sequence starting from the initial geometry (far left panels) with an outer cortical layer of thickness h. The estimated gyrification index (GI) for the initial and gyrified states is shown in the bottom panels. GI is determined here as the ratio of the length of the complete contour (solid blue line) to that of the superficially exposed surface (dotted white line), as in ref. [11].

DOI: 10.1038/NPHYS3632

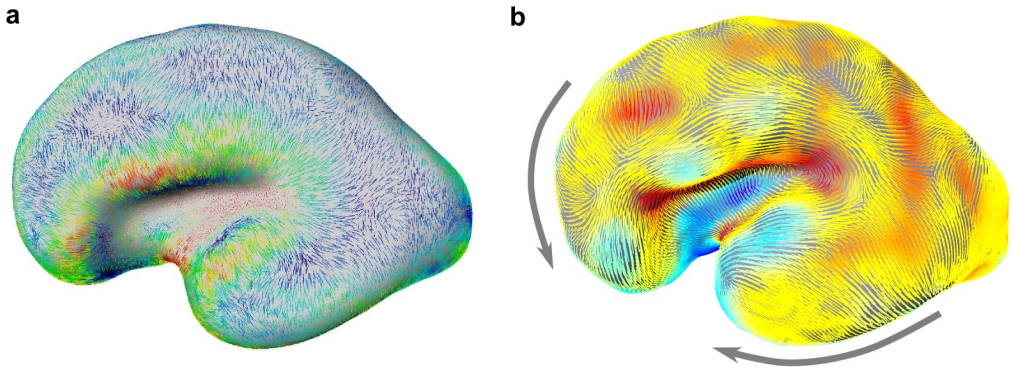

FIG. S3. **Comparison of curvature and stress fields before onset of gyrification.** (**a**) A vector field of maximum curvature in the initial geometry of the simulation. Lines indicate the direction of maximum curvature and color indicates the magnitude of maximum curvature (red = high). (**b**) A vector field of maximum compressive stress before the first sulci form. Lines indicate the direction of the maximum stress and color indicates the magnitude of stress at the surface. Note that the maximum stress is perpendicular to the maximum curvature only in highly curved regions. Arrows illustrate the elongation and bending of the frontal and temporal lobes as a result of cortical expansion.

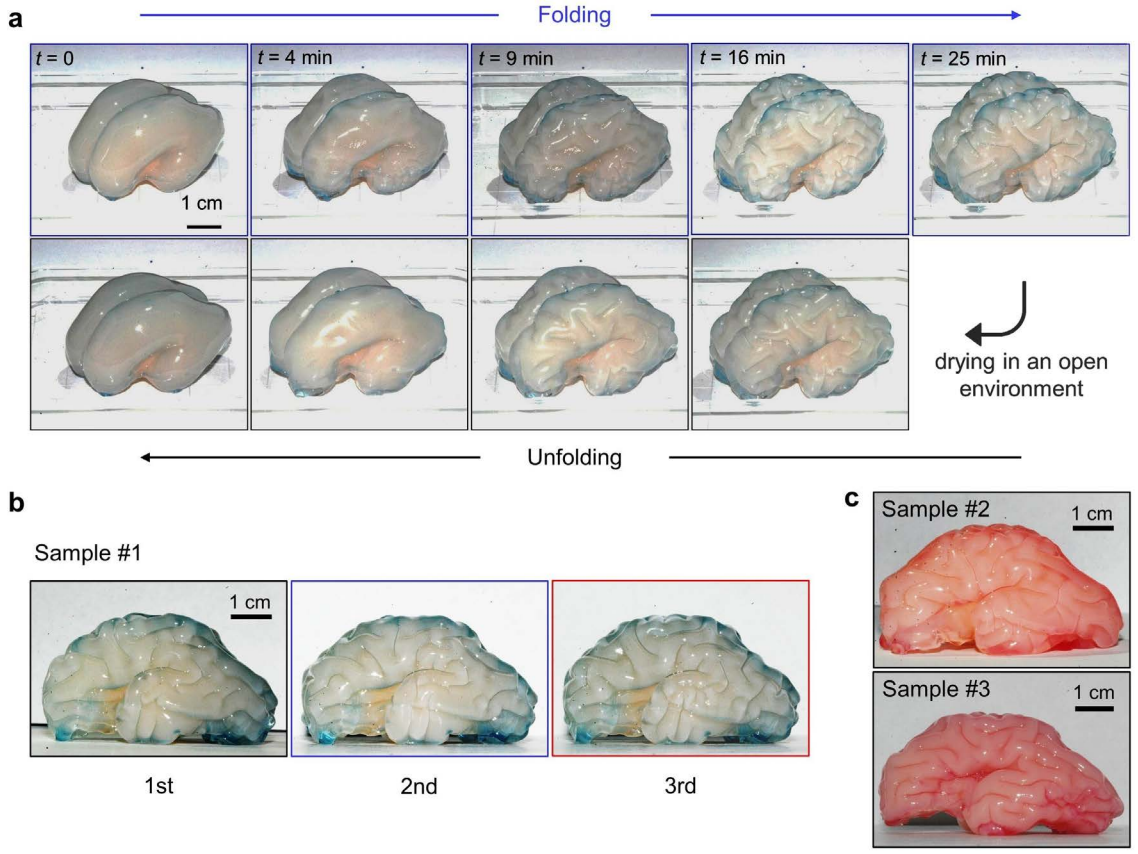

FIG. S4. **Gyrification patterns from physical experiment.** (**a**) Folding and unfolding of a physical gel brain. A comparison of brain morphologies is obtained by first swelling the gel brain in hexanes (folding; top rows) and then drying it in an open environment (unfolding; bottom rows). (**b**) Left-side images obtained from repeated tests with the same gel brain. Each test is conducted after complete drying of the swollen gel (several days) to eliminate any possible memory effect. (**c**) Comparison of the left-side images shown in (**b**) with the two other gel brains prepared with the same experimental protocol but with different colored pigments.

DOI: 10.1038/NPHYS3632

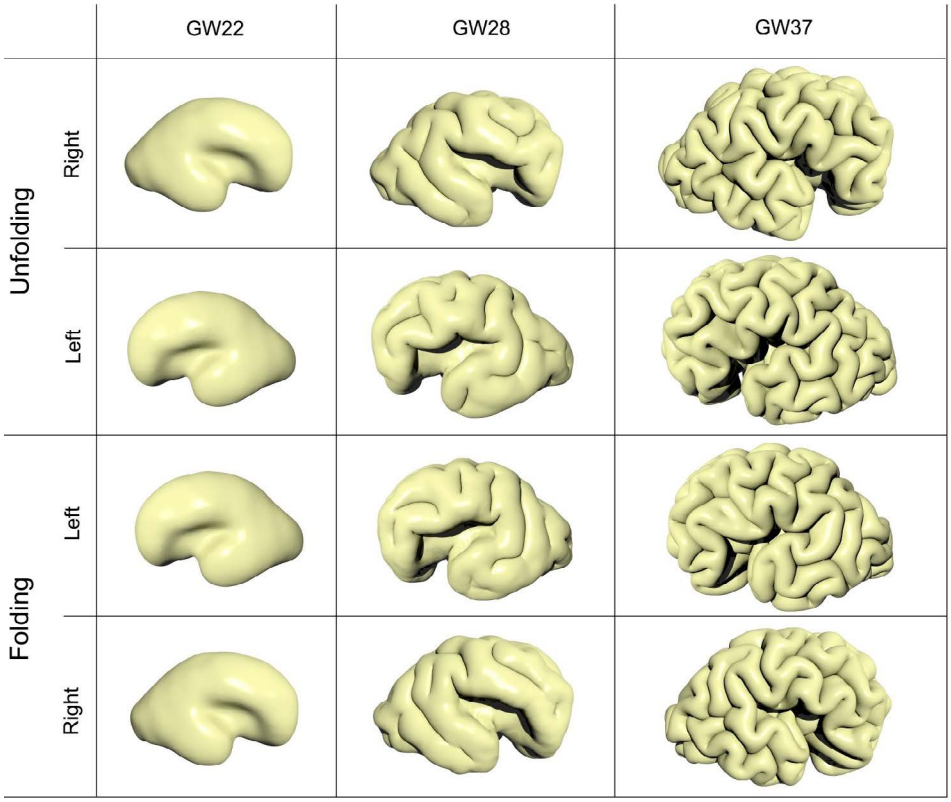

FIG. S5. **Folding and unfolding of a numerical brain.** A comparison of brain morphologies is obtained by unfolding (two rows at top for right and left hemispheres) and folding (two rows at bottom for left and right hemispheres) simulations.

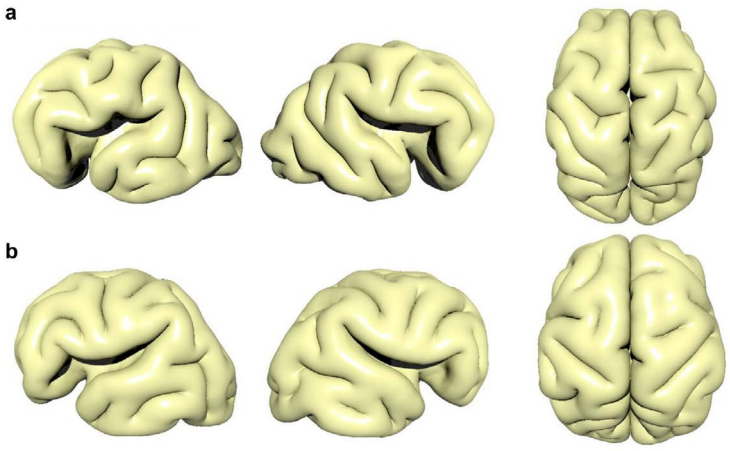

FIG. S6. **Gyrification patterns corresponding to GW 30 on two different simulated brains.** The simulations are performed starting from MR images of two different smooth fetal brains: (**a**) Simulation mesh from a MRI of a GW 22 smooth fetal brain; (**b**) Simulation mesh from a MRI of a GW 23 smooth fetal brain. These simulations were run forward in time.

Movie S1: Growth and folding of a physical gel brain

Movie S2: Growth and folding of a numerical brain

[1] J. Nase, A. Lindner, and C. Creton, *Pattern formation during deformation of a confined viscoelastic layer: From a viscous liquid to a soft elastic solid*, Phys. Rev. Lett. **101**, 074503 (2008).

[2] J. N. Lee, C. Park, and G. M. Whitesides, *Solvent compatibility of poly(dimethylsiloxane)-based microfluidic devices*, Anal. Chem. **75**(23), 6544-6554 (2003).

[3] T. Tallinen, J. Y. Chung, J. S. Biggins, and L. Mahadevan, *Gyrification from constrained cortical expansion*, Proc. Natl. Acad. Sci. U.S.A. **111**(35), 12667-12672 (2014).

[4] A. Stomakhin, R. Howes, C. Schroeder, and J. M. Teran, *Energetically consistent invertible elasticity*, ACM SIGGRAPH Symp. Comp. Anim., 25-32 (2012).

[5] J. Bonet and A. J. Burton, *A simple average nodal pressure tetrahedral element for incompressible and nearly incompressible dynamic explicit applications*, Comm. Num. Meth. Eng. **14**, 437-449 (1998).

[6] C. Ericson, *Real-Time Collision Detection* (Morgan Kaufmann, San Francisco, 2005).

[7] E. Armstrong, A. Scleicher, H. Omran, M. Curtis, and K. Zilles, *The ontogeny of human gyrification*, Cereb. Cortex **5**(1), 56-63 (1995).

[8] G. Xu, A. K. Knutsen, K. Dikranian, C. D. Kroenke, P. V. Bayly, and L. A. Taber, *Axons pull on the brain, but tension does not drive cortical folding*, J. Biomech. Eng. **132**, 071013 (2010).

[9] G. Taubin, *Estimating the tensor of curvature of a surface from a polyhedral approximation*, Fifth International Conference on Computer Vision, Proceedings, 902–907 (1995).

[10] J. Lefèvre, G. Auzias, *Spherical Parameterization for genus zero surfaces using Laplace-Beltrami eigenfunctions*, 2nd conference on Geometric Science of Information, Springer (2015).

[11] K. Zilles, E. Armstrong, A. Scleicher, and H. Kretschmann, *The human pattern in gyrification in the cerebral cortex*, Anat. Embryol. **170**, 173-179 (1988).